Journal of ELECTRONIC MATERIALS, Vol. 47, No. 7, 2018
https://doi.org/10.1007/s11664-018-6262-1

Co-Precipitation Synthesis and Characterization of $SrBi_2Ta_2O_9$ Ceramic

MOHAMED AFQIR,[1,2,3] AMINA TACHAFINE,[2] DIDIER FASQUELLE,[2] MOHAMED ELAATMANI,[1] JEAN-CLAUDE CARRU,[2] ABDELOUAHAD ZEGZOUTI,[1] and MOHAMED DAOUD[1]

1.—Laboratoire des Sciences des Matériaux Inorganiques et leurs Applications, Faculté des Sciences Semlalia, Université Cadi Ayyad, Marrakech, Morocco. 2.—Unité de Dynamique et Structure des Matériaux Moléculaires, Université du Littoral- Côte d'Opale, Calais, France. 3.—e-mail: mohamed.afqir@yahoo.fr

Strontium bismuth tantalate ($SrBi_2Ta_2O_9$) was synthesized by a co-precipitation method. The sample was characterized by x-ray powder diffraction patterns (XRD), Fourier-transform infrared spectroscopy (FTIR) and scanning electron microscopy (SEM). The results of the dielectric properties are reported at room temperature. No secondary phases were found while heating the powder at 850°C and the pure $SrBi_2Ta_2O_9$ phase was formed, as revealed by XRD. The characteristic bands for $SrBi_2Ta_2O_9$ were observed by FTIR at approximately 619 cm^{-1} and 810 cm^{-1}. SEM micrographs for the sample displayed thin plate-like grains. The grain size was less than 1 μm and the crystallite size of about 24 nm. Dielectric response at room temperature shows that the $SrBi_2Ta_2O_9$ ceramic has low loss values, and the flattening of the dielectric constant at higher frequencies. The observed Curie temperature is comparable with those reported in the literature.

Key words: $SrBi_2Ta_2O_9$, co-precipitation, dielectric

INTRODUCTION

Aurivillius phases have the general formula $(Bi_2O_2)^{2+}(A_{n-1}B_nO_{3n+1})^{2-}$, where A stands for a divalent cation (e.g., Ca^{2+}, Ba^{2+}), B for a tetravalent or pentavalent (e.g., Nb^{5+}, Ti^{4+}), and are the perovskite blocks $A_{n-1}B_nO_{3n+1}$.[1] Strontium bismuth tantalate (SBT), $SrBi_2Ta_2O_9$, belongs to the layered perovskite ferroelectrics where the crystal consists of the stacking of alternating layers of Bi_2O_2 and pseudo-perovskite $SrTa_2O_7$ units with double TaO_6 octahedral layers along the *c*-axis.[2] The layered perovskite-like ferroelectric of SBT is attractive for the development of non-volatile random access memories because of its excellent fatigue characteristic.[3] SBT is usually obtained through the mixture of oxides, Bi_2O_3, Ta_2O_5 and $SrCO_3$, which gives large particles and requires high temperatures for the synthesis of this compound.[4] Other methods used for the synthesis of $SrBi_2Ta_2O_9$ ceramic powder are: the sol–gel method,[5] chemical routes,[6] solution combustion technique,[7] and hydrothermal process.[8] A study of many ceramics of the same chemical compound, but synthesized under different conditions, might reveal trends in the crystallite size, which in turn can be related to the properties of the product. For random access memory applications, it is necessary to obtain the $SrBi_2Ta_2O_9$ materials with low dielectric loss, low conductivity and high fatigue properties.[9] To prevent the volatilization of Bi_2O_3 during sintering above 1000°C, which could result in oxygen and bismuth vacancies, it is therefore desirable to dope $SrBi_2Ta_2O_9$ by rare earth elements.[10,11] Meanwhile, an accurate amount of Bi_2O_3 oxide must be added to compensate experimentally for the loss characteristics of the Bi_2O_3 oxide. To our knowledge, it does not resolve many practical physical issues such as the microstructure–property relationship and the physical nature leading to the change of the dielectric

(Received October 15, 2017; accepted March 23, 2018; published online April 3, 2018)

properties of $SrBi_2Ta_2O_9$ ceramics. In this regard, we report a co-precipitation method to obtain $SrBi_2Ta_2O_9$ with sub-micron grain size. X-ray powder diffraction patterns (XRD), Fourier-transform infrared spectroscopy (FTIR) and scanning electron microscopy (SEM) are used to characterize the synthesized material. Dielectric measurements were performed.

EXPERIMENTAL

A flowchart of the co-precipitation procedure used is shown in Fig. 1. A stoichiometric amount of $SrCl_2{\cdot}6H_2O$ (Normatom) was dissolved in distilled water, $Bi(NO)_3{\cdot}5H_2O$ (Fluka Chemika, 99.0%) was dissolved in a minimum amount of dilute HNO_3 (Panreac, 65%) to avoid precipitation of Bi ions, and Ta_2O_5 (Fluka Chemika, 99.9%) was dissolved in a minimum amount of HF (Riedel-de Haën, 40%). The three limpid solutions were mixed together, followed by the addition of KOH (Acros Organics) solution (10 M) until pH = 12 to ensure complete precipitation. The precipitate was filtrated by washing several times with distilled water. After drying in the oven, the precursor was heated in a furnace at 400°C for 12 h, and then at a rate of 5°C/min to 800°C and kept at this temperature for 24 h. The pellet was sintered at 850°C for 12 h. Both sides of the sintered sample were painted with silver paste and fired to form the electrodes.

X'Pert HighScore Plus software (PANalytical) was used to estimate the degree of crystallization. The dried sample was ground with KBr to form a mixture containing 1% mass of the sample, and a small pellet of the mixture was pressed and scanned by FTIR (KBr-pellet; Bruker Vertex 70 DTGS). The microstructure of the sintered pellet was analyzed by SEM with 10 kV of accelerating voltage in a high vacuum. The dielectric properties were investigated at a range from room temperature to 400°C using a LCR meter HP 4284A.

RESULTS AND DISCUSSION

Figure 2a shows the XRD pattern of $SrBi_2Ta_2O_9$ ceramic powder. All Bragg peaks of this sample were found to correspond to the layered perovskite $SrBi_2Ta_2O_9$ crystal structure (JCPDS no 01-070-4062). No pyrochlore phase was found while heating the powder at 800°C. The refined lattice parameters are a = 5.51752 Å ± 0.00085 Å, b = 5.52500 Å ± 0.00023 Å and c = 25.08384 Å ± 0.00203 Å. These parameters are comparable with those reported (a = 5.5146 Å, b = 5.5246 Å and c = 24.9017 Å) in the literature.[12]

Crystallite size and micro-strain were measured according to the method of Williamson and Hall[13,14] (Fig. 2b).

$$\beta \cos\theta = \frac{0.89}{D}\lambda + 4\varepsilon \sin\theta \qquad (1)$$

where β is the integral breadth, D is the crystallite size, (ε) the micro-strain and (θ) the diffracted angle. The reflections with a low intensity of the peaks were excluded from the analysis. The slope corresponds to the strain and the intercept corresponds to the crystallite size. The average crystallite size was $\sim$ 24 nm and micro-strain was about $\sim 7.26 \times 10^{-4}$. The crystallite size/strain deduced from the $\beta\cos\theta$ versus $\sin\theta$ described the formation of nanoparticles.

Figure 3 shows the FTIR spectrum of the $SrBi_2Ta_2O_9$ ceramic powder. The bands at 3452 cm^{-1} and 1630 cm^{-1} are due to water molecules. The bands located at 2387 cm^{-1} can be attributed to CO_2. Bands at 1386 cm^{-1}, 2853 cm^{-1}, and 2929 cm^{-1}

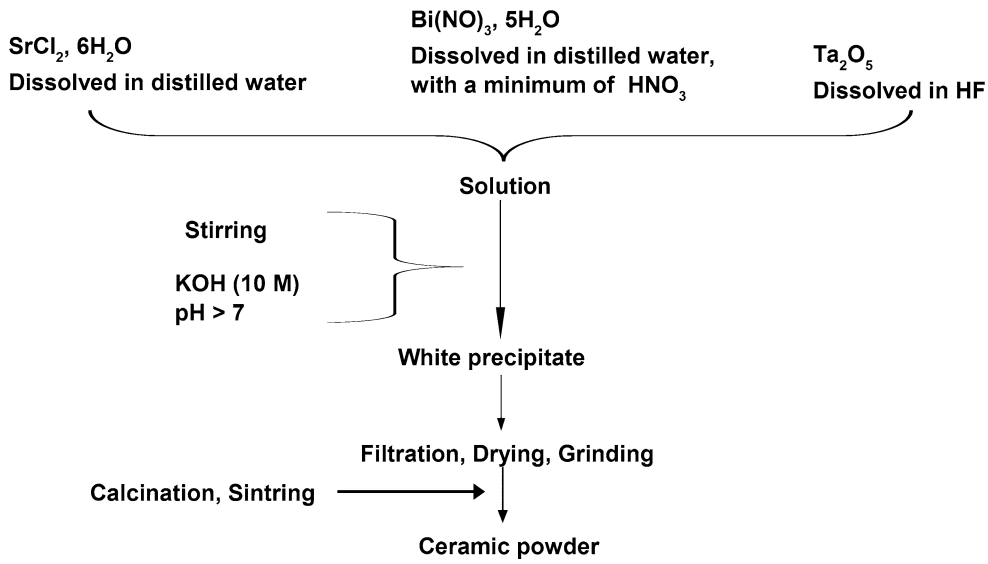

Fig. 1. Flowchart for the preparation of $SrBi_2Ta_2O_9$ powder by co-precipitation.

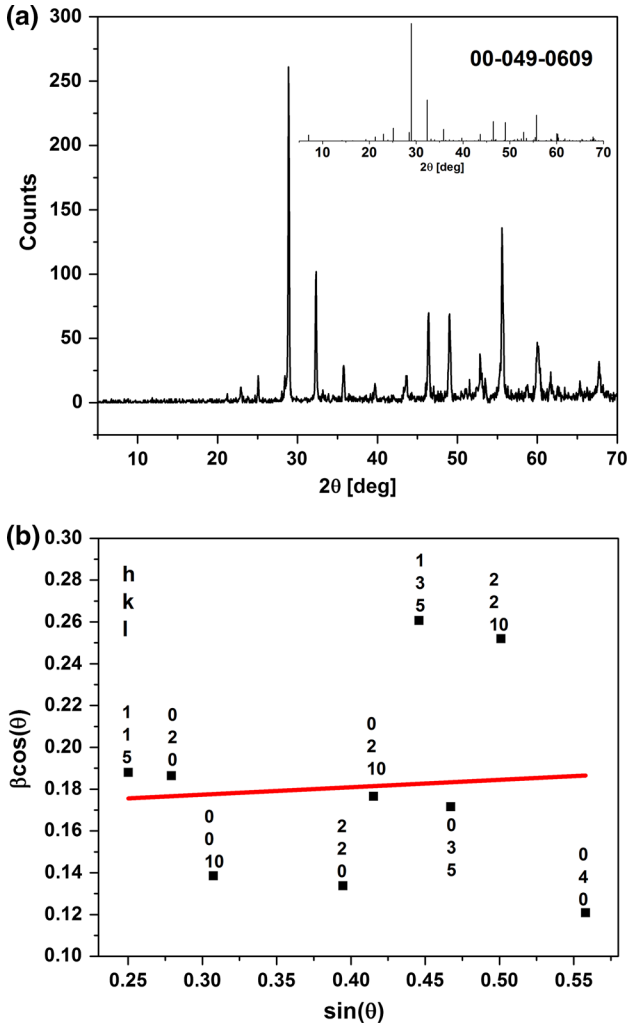

Fig. 2. (a) XRD pattern and (b) corresponding Williamson–Hall plot for $SrBi_2Ta_2O_9$ ceramic powder.

indicate the presence of residual organics, and 619 cm^{-1} and 810 cm^{-1} are expected for octahedral stretching TO_6. These two infrared absorption bands are related to the crystallization of the phase $SrBi_2Ta_2O_9$.[12,14] Also, note there is no presence of residual precursors or unwanted secondary phases at a temperature of 800°C.

Figure 4 shows the cross-sectional microstructure investigated by SEM of $SrBi_2Ta_2O_9$ ceramic. The sintered pellet exhibits less porosity, relatively dense structure, small rod-like and plate-like shaped grains. The plate-lake morphology has been considered to be the characteristic grain growth of Aurivillius microstructures.[15–17] The obtained samples are micro- to nanograined and therefore contain well developed grain boundaries and free surfaces. It has recently been demonstrated that the physical properties of pure and doped fine-grained oxides strongly depend on the presence of defects like interphase boundaries and grain boundaries.[7,14]

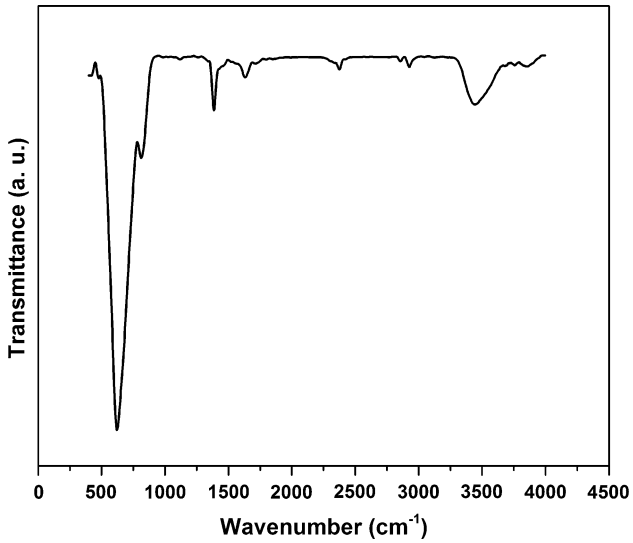

Fig. 3. FTIR spectrum of $SrBi_2Ta_2O_9$ ceramic powder.

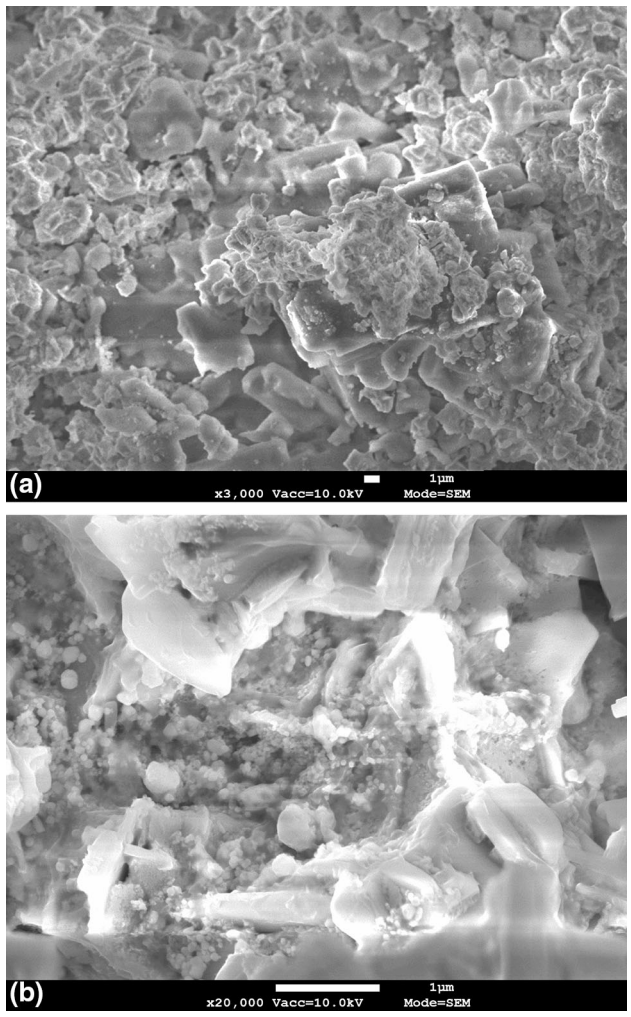

Fig. 4. (a, b) SEM images of $SrBi_2Ta_2O_9$ ceramic.

Figure 5 shows the temperature-dependent dielectric constant (ε') and dielectric loss ($\tan\delta$) for $SrBi_2Ta_2O_9$ ceramic at room temperature. Both the ε' and $\tan\delta$ values decrease with increasing frequency. The dielectric constant decreases significantly with frequency and ranges from 287 to 94 in the frequency range of 100 Hz–10 kHz. In general, for all materials, the dielectric constant continuously decreases with frequency, due to the space charge polarization and interface effect.[17] Another explanation suggests that these observations may be due to the fact that the dipoles cannot follow the rapid variation of the applied field.[15,18] For the analysis of frequencies below 10 kHz down to 1 MHz, ε' remains constant around a value of ~ 86. The dielectric loss is found to be less than ~ 0.005 when measured at 100 kHz, which is lower than those reported from $SrBi_2Ta_2O_9$ ceramics prepared by a solid-state method.[19,20] The frequency dependence of the dielectric properties at room temperature shows low loss values at higher frequencies and the flattening of dielectric constant, which are very desirable in nonvolatile ferroelectric random access memory applications. The plot of the temperature-dependent dielectric constant (ε') and dielectric loss ($\tan\delta$) at different frequencies for $SrBi_2Ta_2O_9$ ceramic is shown in Fig. 6. A Curie temperature is observed at 330°C, which is in good agreement with the reported value (310°C ± 20°C).[17,21] It may also be noted that the values of dielectric loss do not exceed the value of 0.5 over the temperature range of 50–400°C.

As noted in the "Introduction", the $SrBi_2Ta_2O_9$ ceramics suffer from high dielectric loss due to the volatilization of bismuth during the sintering process at temperatures greater than 1000°C. The losses are attributed to increased conduction arising from lattice defects induced through volatilization of the bismuth oxide.[22] With the synthesis conditions described above, the grain sizes are found to be extremely small, and may give rise to resistive and capacitive grain boundaries. As

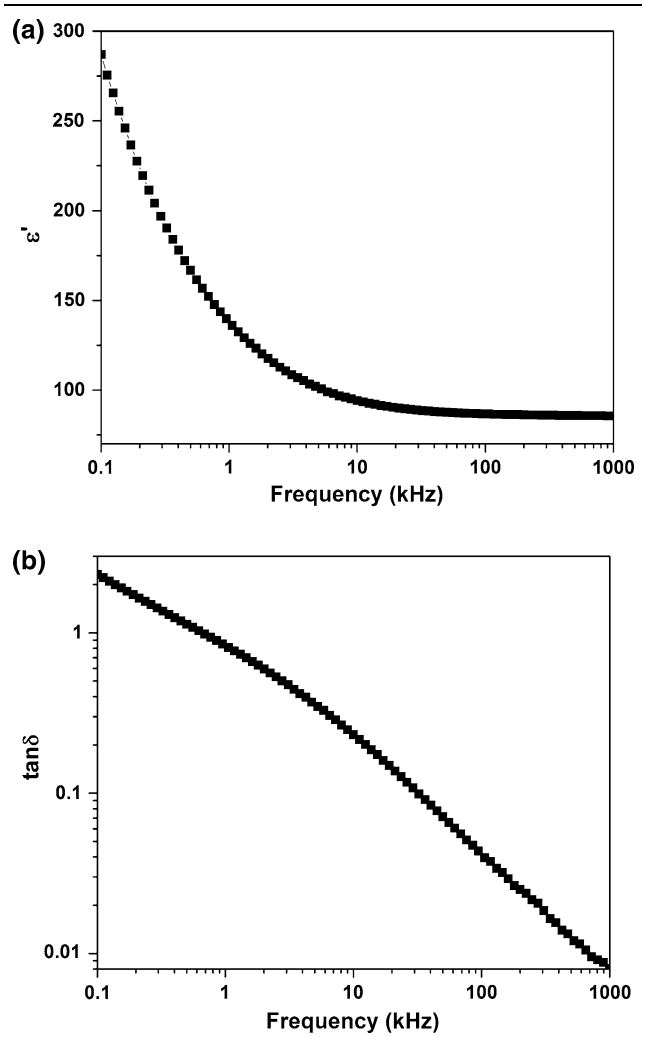

Fig. 5. (a) Frequency dependence of dielectric constant and (b) dielectric loss at room temperature for $SrBi_2Ta_2O_9$ ceramic.

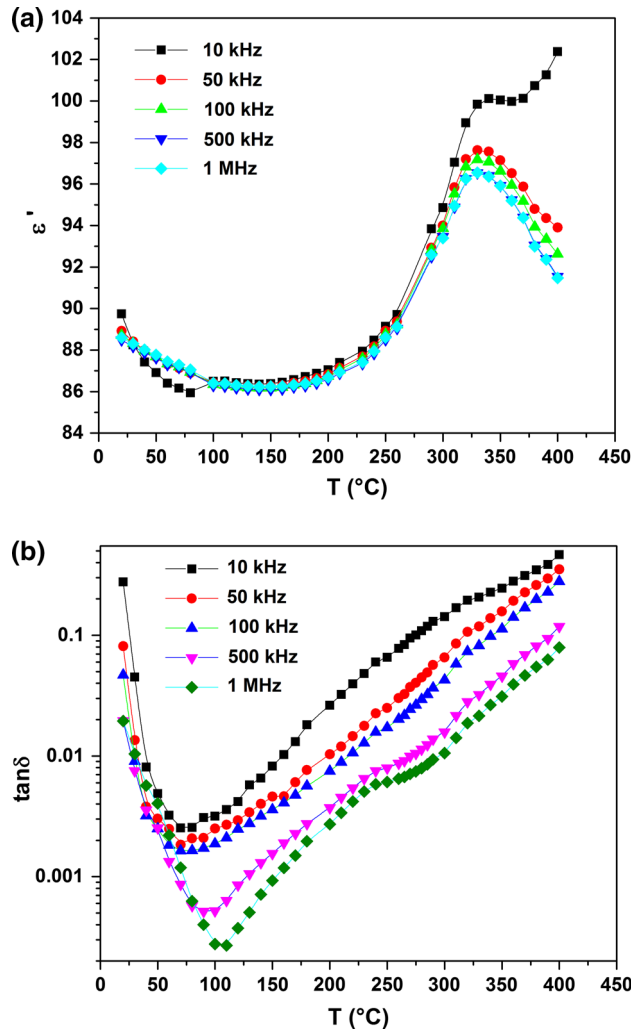

Fig. 6. (a) Temperature-dependent dielectric constant and (b) dielectric loss at different frequencies for $SrBi_2Ta_2O_9$ ceramic.

improved elsewhere,[23,24] the dielectric loss appears to be a strong function of grain size. Thus, the decrease in loss can be understood from the fact that the lower conductivity of the fine-grained ceramics is due to the higher density of resistive grain boundaries. It can be concluded that our ceramic processing conditions may reduce lattice defects, which increases the resistivity and reduces dielectric loss.

CONCLUSION

Nanosized $SrBi_2Ta_2O_9$ ceramic powder was synthesized through a simple co-precipitation method. This process seems to afford a means towards an environmentally friendly and inexpensive aqueous synthesis. The Williamson–Hall method was used to understand the contributions of lattice strain and crystalline size to the XRD peaks. The dielectric properties at room temperature of the proposed material can match those of the $SrBi_2Ta_2O_9$ ceramic prepared by solid-state reaction. The dielectric constant remains constant with a loss of 0.005 at a frequency of 100 kHz. The co-precipitation route for sample preparation shows advantages over the solid-state reaction approach, such as no evidence for bismuth volatilization in the processing condition.

OPEN ACCESS

REFERENCES

1. E.P. Kharitonova and V.I. Voronkova, *Inorg. Mater.* 43, 1340 (2007).
2. V.A. Isupov, *Inorg. Mater.* 42, 1094 (2006).
3. Q.-H. Li, M. Takahashi, T. Horiuchi, S. Wang, and S. Sakai, *Semicond. Sci. Technol.* 23, 45011 (2008).
4. B. Li, L. Li, and X. Wang, *Ceram. Int.* 29, 351 (2003).
5. W. Wang, H. Ke, J. Rao, M. Feng, and Y. Zhou, *J. Alloys Compd.* 504, 367 (2010).
6. A.B. Panda, A. Tarafdar, A. Pathak, and P. Pramanik, *Ceram. Int.* 30, 715 (2004).
7. F.F. Oliveira, S. Da Dalt, V.C. Sousa, and C.P. Bergmann, *Powder Technol.* 225, 239 (2012).
8. H. Wang, J. Liu, M. Zhu, B. Wang, and H. Yan, *Mater. Lett.* 57, 2371 (2003).
9. P. Nayak, T. Badapanda, and S. Panigrahi, *J. Mater. Sci. Mater. Electron.* 28, 625 (2017).
10. I. Coondoo and A.K. Jha, *Mater. Lett.* 63, 48 (2009).
11. V. Senthil, *J. Mater. Sci. Mater. Electron.* 27, 1602 (2016).
12. I. Coondoo, A.K. Jha, and S.K. Agarwal, *Ceram. Int.* 33, 41 (2007).
13. H. Mändar, J. Felsche, V. Mikli, and T. Vajakas, *J. Appl. Crystallogr.* 32, 345 (1999).
14. S. Thankachan, B.P. Jacob, S. Xavier, and E.M. Mohammed, *Phys. Scr.* 87, 025701 (2013).
15. B.R. Kannan and B.H. Venkataraman, *J. Mater. Sci. Mater. Electron.* 25, 4943 (2014).
16. D. Kajewski, Z. Ujma, K. Szot, and M. Pawełczyk, *Ceram. Int.* 35, 2351 (2009).
17. G.S. Murugan and K.B.R. Varma, *J. Electroceramics* 8, 37 (2002).
18. C.H. Lu and S.K. Saha, *Mater. Res. Bull.* 35, 2135 (2000).
19. V. Senthil, T. Badapanda, A. Chandrabose, and S. Panigrahi, *Mater. Lett.* 159, 138 (2015).
20. M. Afqir, A. Tachafine, D. Fasquelle, M. Elaatmani, J.-C. Carru, A. Zegzouti, and M. Daoud, *Open J. Phys. Chem.* 6, 42 (2016).
21. I. Coondoo, A.K. Jha, and S.K. Agarwal, *J. Eur. Ceram. Soc.* 27, 253 (2007).
22. S.U. Jan, A. Zeb, and S.J. Milne, *J. Eur. Ceram. Soc.* 36, 2713 (2016).
23. G. Liu, S. Zhang, W. Jiang, and W. Cao, *Mater. Sci. Eng. R* 89, 1 (2015).
24. E.P. Papadakis, *J. Acoust. Soc. Am.* 33, 1616 (1961).